The effects of curing process on the damage behavior of additively manufactured fiber-reinforced thermosetting composites

Sina Niazi[1], Aimane Najmeddine[1] and Maryam Shakiba[2*]

[1]Department of Civil and Environmental Engineering, Virginia Tech, Blacksburg, VA, 24061, USA.
[2]Smead Aerospace Engineering Sciences Department, University of Colorado, Boulder, CO, 80303, USA.

*Corresponding author(s). E-mail(s): maryam.shakiba@colorado.edu;

Abstract

This work investigates the effects of high-temperature curing processes on the stress-strain and failure responses of additively manufactured aligned discontinuous fiber-reinforced composites (DFRCs). A micromechanical framework is used for finite element simulation of damage and failure in the three-dimensional (3-D) representation of the DFRCs under mechanical and thermal loadings. Accurate constitutive equations are utilized to explicitly consider the fibers, matrix, and fiber/matrix interfaces within the composite's microstructure. The coupled thermo-mechanical analysis available on the commercial nonlinear finite element software ABAQUS is used to accurately simulate the response of the studied DFRC when exposed to different curing temperatures and mechanical loading. All material and geometrical parameters of the microstructural representation are defined based on a recently developed 3-D printed aligned discontinuous fiber-reinforced thermosetting polymer. The curing-induced thermal residual stresses and damage are then simulated and validated against the experimental data. The effects of different curing processes on the initiation and propagation of different damage types and on the stress-strain response up to and including final failure are predicted. Also, the impact of the perfect versus cohesive interfacial bonding on the DFRC's performance is examined. This work

reveals that the DFRCs' responses are significantly affected when residual thermal stresses due to curing are considered, providing guidance for better design, manufacturing, and analysis of such composites.

Keywords: Finite element simulation, additive manufacturing, carbon fiber-reinforced thermosetting composites, curing process, thermal residual stress, damage, failure

1 Introduction

Recent advancements in developing thermoset polymer composition and injection technologies have enabled the additive manufacturing of discontinuous fiber-reinforced composites (DFRCs) with highly aligned fibers (e.g., [1–4]). One of these techniques uses the direct write method, where material melting is not required for printing thermosetting polymers, and the entire structure is printed at room temperature. Thermal curing is then applied, sometimes even up to the temperature of 220°C, in a secondary process to achieving 100% degree of cure [4]. The secondary process for thermal curing simplifies the entire manufacturing procedure and reduces the dependence of the mechanical properties on thermal printing history, and spatial heating path [2, 4]. However, the curing process still induces residual thermal stresses due to the mismatch in the coefficients of thermal expansion (CTE) during heating and cooling from the curing temperature to room temperature. The residual stresses can be high enough to initiate microcracks and damage prior to mechanical loading. The microcracks then coalesce, leading to the formation of macrocracks, reducing the overall strength, and consequently compromising the composite's performance (e.g., [5–7]). Therefore, it is critical to understand and accurately predict residual thermal stresses' influence on the composite's performance.

Residual thermal stresses in carbon fiber-reinforced composites (CFRCs) have been investigated by various experimental, analytical, and computational methodologies. Destructive and non-destructive experimental techniques were conducted to investigate the effects of residual thermal stresses [8–10]. However, such techniques are too complicated, expensive, and incapable of quantitatively demonstrating the influence of the residual stresses on the damage initiation and propagation in composites. Moreover, these residual stresses at the macro-scale have been predicted by the classical laminate theory or other analytical methods [11–15]. Nonetheless, analytical methods cannot calculate the stress, strain, and damage fields at micro- and meso-scales [16, 17]. Therefore, computational techniques, such as finite element methods (FEMs), are necessary to calculate the residual thermal stress and strain at the micro-scale, leading to precise predictions of stress concentration, deformation, damage onset, and propagation.

FEMs have been extensively utilized to study residual thermal stresses in CFRCs in the literature (e.g., [5–7, 18–24]). Most of these works examined

the effect of the curing-induced residual stresses on the transverse response of CFRCs through two-dimensional (2-D) simulations. Among the literature, Yuan et al. [22] used three-dimensional (3-D) micromechanical models to investigate the effects of temperature and macro residual stresses on the evolution of micro residual stresses, but not on damage initiation and evolution. Moreover, in most of these works, the influence of fiber/matrix interfaces on the composite's performance has been neglected. Several studies had emphasized on the critical effect of fiber/matrix interface properties on the response of CFRCs (e.g., [25, 26]). Among the above works, references [5, 7, 20] incorporated the effect of fiber/matrix interfaces, but through 2-D simulations. Consequently, a reliable validation of the composite's response against experimental data has seldom been found in the literature. Therefore, a comprehensive 3-D micromechanical model that incorporates the fiber/matrix interfaces is required to accurately investigate the effects of curing-induced residual stresses on the mechanical response and failure behavior of CFRCs.

Sepasdar et al. [27] proposed a micromechanical model within an FEM framework to simulate damage and failure in the 3-D representation of additively manufactured aligned DFRCs under pure mechanical loading. This numerical framework utilized accurate constitutive equations to simulate the fibers, matrix, and fiber/matrix interfaces explicitly. A cohesive zone model (CZM) was used to examine the possible interfacial debonding. All material and geometrical parameters were defined based on the recently developed 3-D printed DFRC by Pierson et al. [4] as the composite of interest. In [27], the accuracy of the micromechanical framework was verified against the experimental results. It was also shown that the proposed framework could accurately simulate various aspects of the mechanical response, including the failure pattern and the stress-strain behavior. However, residual thermal stresses were not taken into account.

The present work aims to study the effects of curing-induced residual thermal stresses on the mechanical response and the failure behavior of DFRCs. To this end, building upon [27], a coupled thermo-mechanical constitutive equation is used through the commercially available nonlinear FEM software ABAQUS [28]. The effects of different curing processes on the onset and evolution of different damage types and the stress-strain response up to and including final failure are simulated. Also, the impact of perfect and cohesive fiber/matrix interfacial bondings on the DFRC's performance is compared. This study provides guidance on the curing procedure of additively manufactured aligned DFRCs, eventually leading to better design, manufacturing, and analysis of such composites.

The rest of this paper is organized as follows. Section 2 presents the numerical simulation framework including the thermo-mechanical analysis approach, the 3-D micromechanical model, and constitutive equations for simulating the response of fibers, matrix, and fiber/matrix interfaces. Section 3 explains material properties of the DFRC's constituents. Section 4 validates our simulation results against experimental data for the studied composite's response.

Section 5 examines the effects of thermal curing process. Parametric studies for several numerical tests are performed and discussed in Section 6. Finally, conclusions and future work are given in Section 7.

2 Numerical simulation framework

This section explains the thermo-mechanical framework, the micromechanical model, and constitutive equations used in this work to study the effects of curing-induced residual stresses on the mechanical response and failure behavior of the DFRC.

2.1 Thermo-mechanical analysis of DFRC

Residual stresses in fiber-reinforced polymer–matrix composites are caused by two major contributions: (1) volume shrinkage of matrix resulting from the chemical reaction, i.e., cross-link polymerization, during curing at an elevated temperature, (2) different thermal contraction of matrix and fiber due to the mismatch in their CTEs after cooling from the curing temperature to room temperature. The contribution of the chemical shrinkage of the matrix to the overall residual stress was found to be relatively small [18]. The typical range of 2–7% volumetric chemical shrinkage was reported in the literature for epoxy systems [24, 29–31]. The fibers do not undergo any chemical contraction during curing [18, 19]. Therefore, the residual stress induced by the small contribution of the chemical shrinkage was neglected in most literature (e.g., [5, 32]). Following these works, we also assume that the residual stress is merely induced by the second mechanism described above. Therefore, the total strain can be expressed as [18]

$$\mathrm{d}\epsilon_{ij} = \mathrm{d}e_{ij} + \alpha \Delta T \delta_{ij} \tag{1}$$

where $\mathrm{d}\epsilon_{ij}$ (with $i, j = 1,2,3$) is the total strain increment, $\mathrm{d}e_{ij}$ is the elastic strain increment, α is the coefficient of thermal expansion, δ_{ij} is the Kronecker delta, and ΔT is the temperature change.

In the present work, the following two steps were subsequently performed to analyze the influence of thermal residual stress:

- First, a curing process is followed by a cooling process to room temperature in the absence of external mechanical loading.
- Second, an external displacement-controlled loading was applied at room temperature until the sample fully broke.

These subsequent steps denote a one-way coupled thermo-mechanical analysis in which the thermal field affects the mechanical field. The illustration of the applied temperature and mechanical load in our study is schematically shown in Figure 1.

The coupled thermo-mechanical constitutive equation available in ABAQUS/Standard was utilized to accurately simulate the response of the 3-D microstructural representation. The analysis requires the existence of elements

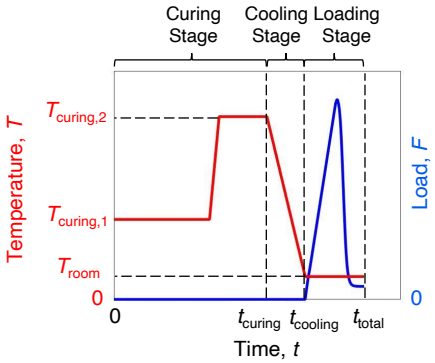

Fig. 1 Schematic illustration of the variations of temperature and mechanical load during the simulation time in our thermo-mechanical analysis.

with both temperature and displacement degrees of freedom [28]. The temperatures were integrated using a backward-difference scheme, and the nonlinear coupled system was solved using the exact implementation of Newton's method [28]. In the following two sections, we first present the micromechanical model for simulating the mechanical response and failure behavior in the 3-D representation of the DFRC. Second, we explain the constitutive equations used for each constituent to describe their mechanical responses, including their failure behavior.

2.2 3-D micromechanical model of DFRC

This section summarizes the 3-D micromechanical model, which was developed and validated by [27] for simulating the aligned DFRC. The overview of the micromechanical model is illustrated in Figure 2. The micromechanical model contains unidirectional and discontinuous carbon fibers of 5 μm diameter with varying aspect ratios embedded within a modified thermosetting epoxy matrix (base ink). Fibers were randomly distributed along the z axis and uniformly distributed along the directions transverse to the fibers' axis (x and y). It should be noted that the fibers' distribution in the transverse directions was known to affect the composites' response only under transverse loading, especially when the fiber volume fraction is low [25, 33, 34]. Since this work investigates the composite's mechanical response under longitudinal tension along the fibers, a uniform transverse distribution of fibers was assumed.

As seen in Figure 2, two linear matrix expansions were incorporated at both ends of the fiber-reinforced region to minimize the impacts of the imposed boundary conditions on the mechanical response and failure mode. Also, the portions of the fiber-reinforced regions next to each end were considered to be linear to prevent a premature failure, normally initiating at the intersections of the fiber-reinforced region and the matrix expansions. The micromechanical model was subjected to longitudinal tension by restraining the displacements of an end (i.e., at z =0) while applying displacement to the opposing end in the

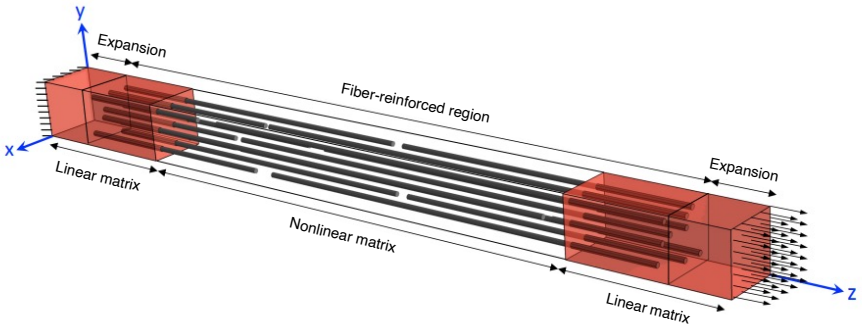

Fig. 2 Schematic illustration of the proposed micromechanical model: overall geometry and boundary conditions.

direction along the fibers' axis (i.e., at $z = L$, where L is the model's dimension along z axis). The strain was evaluated only based on the elongation of the fiber-reinforced region's length.

The location and aspect ratio of the fibers were randomly generated such that the target fibers' volume fraction of 5.5% and the intermediate fibers' aspect ratios (FARs) of around 50 (i.e., the cases for 3-D printed DFRCs) were achieved. The values of the volume fraction and distribution of the FARs were taken from the experimental work of [4]. This micromechanical model was shown to be suitable for studying damage propagation, and failure in 3-D printed aligned DFRCs under longitudinal loading. According to the size sensitivity analysis conducted in [27], optimum microstructural representation dimensions provided a sufficiently large cross-sectional area and length to simulate the mechanical response of the composite accurately and was utilized in the analyses in this study. For more details of the micromechanical model and the procedure for its random generation, the readers are referred to [27].

The computational efficiency of the proposed micromechanical framework relies on the geometrical dimensions, particularly on FARs. The proposed framework performs ideally for investigating composites with intermediate FARs because the simulations can be run using a computer with an ordinary multi-core processor. The efficiency of the proposed framework in studying composites with large FARs is contingent upon additional computational resources.

2.3 Constitutive equations

The constitutive equations for each constituent were defined so that they can properly describe the mechanical response of components in the composite of interest, i.e., 3-D printed DFRC in [4]. The following subsections describe the constitutive equations used to simulate fiber, matrix, and fiber/matrix interface.

2.3.1 Fiber

A transversely isotropic elastic constitutive equation was considered for the fibers. According to the experimental observations, fiber breakage rarely occurs since the fibers are of intermediate length ($FARs \approx 50$) [4].

2.3.2 Matrix

The matrix was analyzed using the plasticity damage constitutive framework initially proposed by Lubliner et al. [35] and later modified by Lee and Fenves [36]. This damage constitutive framework was initially proposed for concrete; however, it has been proven accurate for other quasi-brittle materials, including thermosetting epoxies [37–40]. The constitutive damage equation employs a Drucker-Prager hyperbolic function as the plastic-flow potential, accounting for the pressure dependency of brittle materials through an angle of internal friction ϕ_m.

Based on an experimental tensile test, the constitutive behavior of the matrix was observed to be linear before brittle fracture [4]. Therefore, a bi-linear stress-strain behavior was assumed for the matrix with a Young's modulus E_m, a Poisson's ratio ν_m, and strength σ_m. The post-failure response was assumed to follow a linear decay from the yield strain ϵ_m until the final strain, i.e., the effective plastic strain at the complete failure ϵ_{pl}^{f}, was reached. After the final strain, a residual resistance of $0.01 \times \sigma_m$ was specified [28]. The reason for the consideration of the residual resistance was that the formulation of the damage constitutive framework does not allow the resistance to become zero. Figure 3(a) schematically illustrates the constitutive stress-strain curve for the matrix. The softening portion of the constitutive stress-strain curve is defined based on cracking strain, ϵ_{cr}, as

$$\epsilon_{cr} = \epsilon_{pl} + \frac{d}{1-d}\frac{\sigma_m}{E_m} \tag{2}$$

where ϵ_{pl} is the effective plastic strain and d is the damage variable with values between 0 and 1 corresponding to the cases of the undamaged and fully-damaged loading stages, respectively (see Figure 3(a)). The alleviated mesh dependency in the damage constitutive framework is explained in Appendix A.

The constitutive responses under tension and compression were considered the same for the matrix of interest in this work. This assumption was justified by realizing that the fiber volume fraction is low, and thus, the type of induced stresses in the matrix are mainly tensile for the case of tensile loading along the fibers' axis [27].

2.3.3 Fiber/matrix interface

A bilinear CZM was used to simulate the fiber/matrix interfaces. In the CZM, a penalty contact was assumed for the interfaces before the traction exceeds a specified interface strength, σ_c, and a critical opening displacement, δ_c (see Figure 3(b)). As illustrated in Figure 3(b), the area below the the bilinear

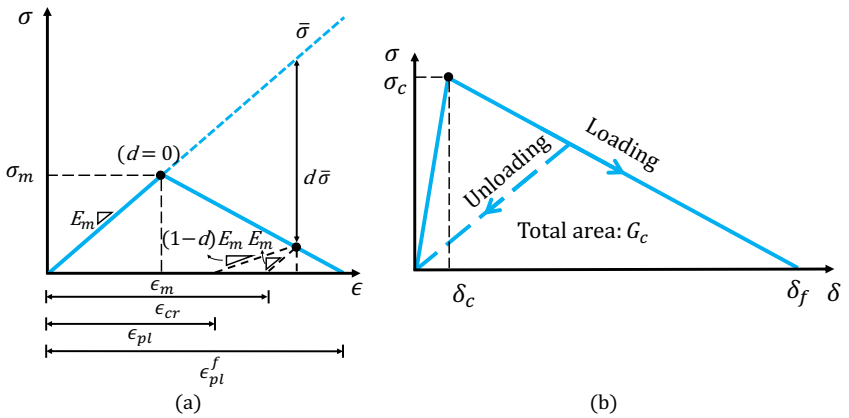

Fig. 3 Schematic illustrations of (a) the constitutive stress-strain curve for the matrix, and (b) the bilinear traction-separation law for the fiber/matrix interfaces.

traction-separation law is equal to the interfacial fracture toughness, G_c. CZMs can sometimes prevent the convergence of the iterative method in the FEM solver by causing infinite iterations [41]. To overcome the convergence difficulty, the viscous regularization method was used, which introduces the addition of an artificial viscosity to the cohesive law [42]. To minimize the effect of the viscous regularization on the accuracy, the viscosity parameter was chosen to be the smallest possible value [28, 41].

3 Material properties of the DFRC's constituents

In this section, material properties used in our thermo-mechanical analysis are provided. The full list of thermo-mechanical properties associated with the fiber and matrix constituents of the DFRC is presented in Table 1. The subscripts m and f in this table refer to the matrix and the fiber, respectively. The properties associated with the thermal response of the fiber and the matrix were taken from [43]. These properties include ρ, C, α, and K, which are density, specific heat, coefficient of thermal expansion, and thermal conductivity, respectively.

The elastic properties associated with the carbon fiber were adapted from [44]. These properties contain E, G, and ν, which are Young's modulus, shear modulus, and Poisson's ratio, respectively. In Table 1, the subscripts 1 and 2 represent the out-of-plane (i.e., along the fibers' axis) and in-plane directions (i.e., transverse to the fibers' axis), respectively, and the subscript 3 denotes the direction perpendicular to the 1 and 2 directions. Note that ν_{23} for the fiber can be calculated by $\frac{E_2}{2G_{23}} - 1$, which is approximately equal to 0.4.

We then calibrate the plasticity damage constitutive framework for the matrix's behavior against the experimental data. The comparison between the

Table 1 Thermo-mechanical properties associated with the fiber and the matrix.

Epoxy Matrix		**Carbon Fiber**	
ρ_m (T/mm^3)	1.2×10^{-9}	ρ_f (T/mm^3)	1.76×10^{-9}
C_m (mJ/T °C)	1×10^{9}	C_f (mJ/T °C)	7.94×10^{8}
α_m (/°C)	4.5×10^{-5}	$\alpha_{f,1}$ (/°C)	-7×10^{-7}
		$\alpha_{f,2}$ and $\alpha_{f,3}$ (/°C)	1.2×10^{-5}
K_m (mJ/mm·s·°C)	0.5	K_f (mJ/mm·s·°C)	10.45
E_m (GPa)	3.25	E_1 (GPa)	233
ν_m	0.3	E_2 (GPa)	23.1
σ_m (MPa)	65	G_{12} (GPa)	8.96
ϕ_m	35	G_{23} (GPa)	8.27
ϵ_m	0.02	ν_{12}	0.2

numerically and experimentally measured stress-strain responses of the matrix (base ink) is illustrated in Figure 4. This figure demonstrates the performance of the employed constitutive behavior in accurately simulating the matrix's mechanical-only response. It should be mentioned that the effect of the thermal curing process on the matrix's response was not considered here. In this figure, the stress of 0.65 MPa after the sudden drop is obtained because of the prescribed residual resistance of $0.01 \times \sigma_m$.

Due to the composite's configuration and the specific loading scenario in this work, the fiber/matrix interface debonding is mainly of mode II (i.e., tangential, occurring along the fibers) or mode I (i.e., normal, occurring at the fibers' tips). Mix-mode debonding scenarios are highly unlikely, and thus, not dominant. Moreover, since the total areas of fibers' tips are significantly smaller than the total lateral areas, the contribution of mode II debonding in the mechanical response is more significant. Hence, both mode I and II debonding were simulated using the same CZM with properties evaluated based on the mode II debonding [27]. For the fiber/matrix interface, the interfacial strength, σ_c, and the interfacial fracture toughness, G_c, were 50 MPa and 150 N/m, respectively (see Figure 3(b)). These values were calibrated based on the experimental results of the composite such that the desired tensile strength and failure pattern were attained [27]. The critical opening displacement, δ_c, was chosen to be sufficiently small to ensure the continuity condition [34].

It should be mentioned that the mechanical properties of the DFRC's constituents were assumed to be temperature-independent following the standard approach in the literature (e.g., see [43]).

4 Validation versus experimental data

In this section, first, our results for the global mechanical response of the DFRC are quantitatively validated against experimental data of [4]. Then, the qualitative validation of our results for the damage propagation against the experimental observations is presented.

In our previous work [27], a sensitivity analysis on the size of the microstructural representation of the composite of interest that can simulate

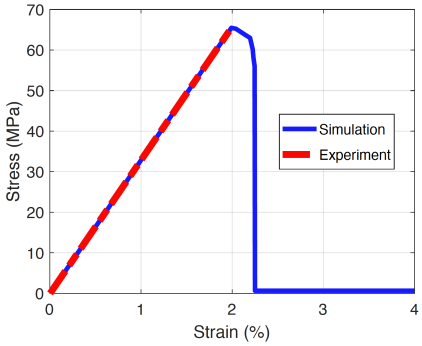

Fig. 4 Comparison of the numerical and experimental results for the stress-strain response of the matrix (base ink).

the mechanical response and failure behavior accurately was conducted. In this study, we used the verified size to conduct thermo-mechanical analysis. This micromechanical representation is illustrated in Figure 5.

The temperature history used in our simulations is illustrated in Figure 6. Based on the experiments of [4], the temperature history during curing is 100°C for 15 h followed by 220°C for 2 h. These actual times were proportionately scaled for the pseudo time of 1 s, as shown in Figure 6. During the cooling process, the temperature was considered to decrease linearly to room temperature.

Note that the temperature history was applied on the outer surfaces of the composite. Additionally, the prescribed temperature was imposed to the inside of the composite at the beginning of the simulation. Therefore, the temperature was homogeneous within the composite at the beginning of the simulation. As long as the prescribed temperature was kept constant, the temperature within the composite was homogeneous. When the prescribed temperature increased, due to the temperature difference between the outside and inside of the composite and consequently the generated heat diffusion, the temperature distribution at the composite's microscale was not homogeneous.

After the cooling process, the mechanical loading of the displacement-controlled type was exerted while the temperature remained constant, i.e. equal to the room temperature, until the end of the simulation time.

4.1 Quantitative validation of the global mechanical response

This section validates the global mechanical response obtained by thermo-mechanical simulations against those from the experiment of [4]. Twenty random realizations of the micromechanical model were simulated. Figure 7(a) demonstrates a sample of the stress-strain response obtained by the thermo-mechanical framework in this work against the representative stress-strain plot from [4]. Figure 7(b) illustrates the statistical measurements of the simulations

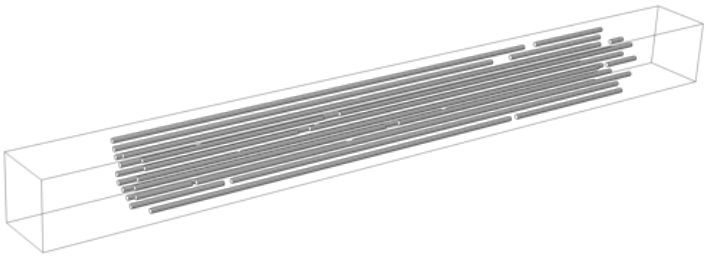

Fig. 5 The model used as the microstructural representation of the DFRC.

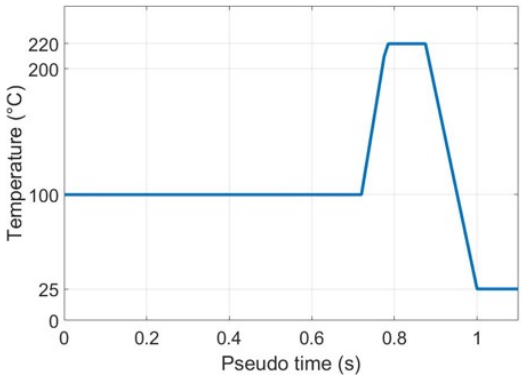

Fig. 6 Temperature history during and after curing, based on the experiments in [4].

versus experimental data. It can be seen that an excellent agreement is found between the simulations' results and the experimental data. As seen in this figure, the tensile strengths calculated from different microstructural realizations of the composite are within the range of experimental data of [4] (shown in shaded blue). The average of the strength calculated from the simulations of different microstructural realizations is very close to that of the experimental data (shown in red dashed line), with a 2% relative error.

4.2 Qualitative validation of the propagated damage and failure

This section presents the evolution of damage and failure within the DFRC after applying the mechanical loading and then validates our results against experimental observations. Figure 8 illustrates the evolution of damage and failure within the studied composite. In this figure, the damage maps corresponding to three representative applied strain levels up to the maximum stress in the stress-strain curve are displayed to visualize how damage and failure evolve within the DFRC. The interface bonding and the matrix damage are respectively exhibited in blue and red colors in this figure and other figures of this paper that include failure maps. As seen in this figure, in addition to

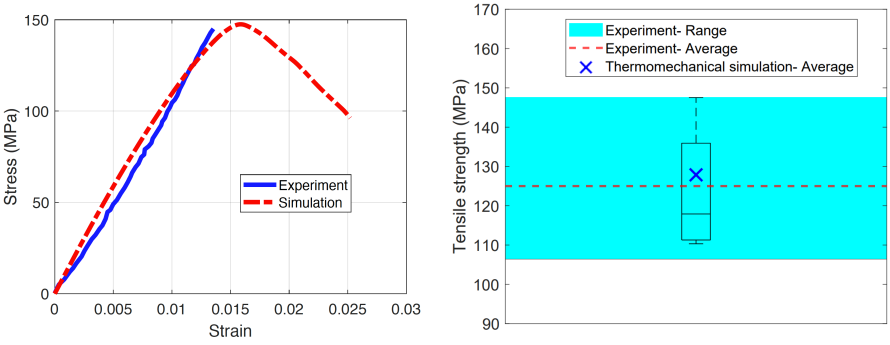

(a) (b)

Fig. 7 Comparisons of (a) the overall stress-strain response, and (b) the overall tensile strength obtained from various microstructural realizations against the experimental data of [4].

the interface bonding, the matrix damage was later initiated and propagated greatly in the composite. It should be noted that in some literature, matrix damage and interface debonding are referred to, with different terminologies, as "cohesive fracture" and "adhesive fracture", respectively (e.g., [45]).

The observed failure modes in Figure 8 are consistent with the experimental images in [4]. Figure 9 shows the microscopic images of fracture surfaces after applying mechanical loading and demonstrates the existence of two damage types of matrix damage and interface debonding in the studied composite. This figure can be served as a qualitative validation of our obtained results for the existence of two damage types in the studied composite. Also, similar experimental microscopic images can be found in the literature that indicate the initiated and fully propagated stages of different damage types in carbon fiber-reinforced thermosetting composites (e.g., see Fig. 6 of [45]).

5 The impacts of thermal curing process

It is critical to investigate to what extent the consideration of the thermal curing process affects the global mechanical response, including the failure response, of the studied composite. Hence, in the next two sections, we first compare thermo-mechanical versus mechanical-only analyses and then study the thermal residual stresses and damage generated prior to the mechanical loading and merely due to the curing procedure.

5.1 Comparison of thermo-mechanical versus mechanical-only analyses

This section compares the thermo-mechanical and mechanical-only analyses of the DFRC's response. Similar to the previous section, twenty realizations of the micromechanical representations of the DFRC were utilized in the analyses to effectively represent the studied composite's response.

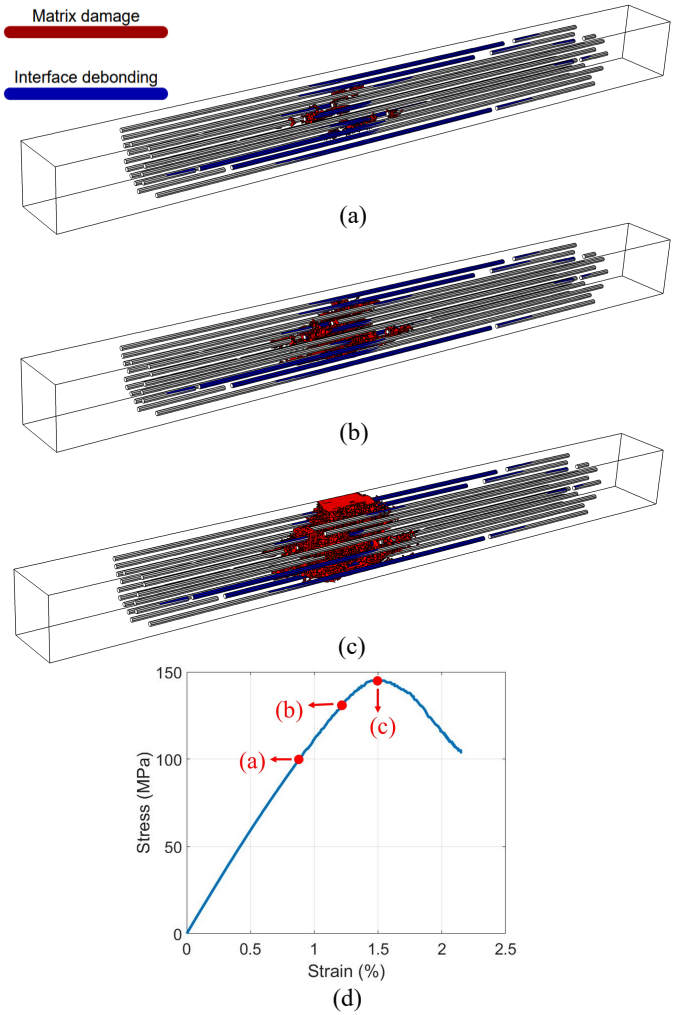

Fig. 8 In (a)-(c): evolution of damage and failure within the DFRC at different applied strain levels. In (d): the stress-strain curve showing the loading stages corresponding to the damage maps of (a)-(c).

Two possible curing scenarios were considered in the thermo-mechanical analysis to study the influence of different thermal curing processes. As illustrated in Figure 10: the first curing process was according to the experiment of [4], where the thermal curing is mostly conducted at 100°C followed by heating to 220°C and keeping at this temperature for a short time, called the actual curing; and the second curing process was conducted at the constant curing temperature of 220°C, called the isothermal curing. The two curing processes were followed by the same cooling process, i.e., cooling from the same curing temperature to room temperature.

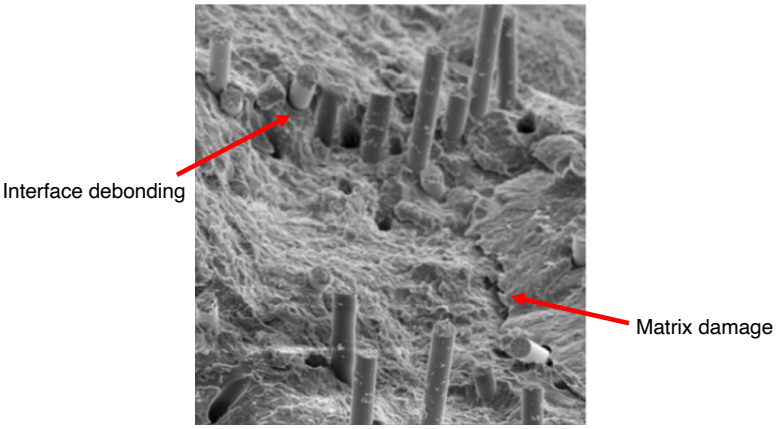

Fig. 9 A scanning electron microscope (SEM) image of fracture surfaces in the experiment of [4].

The applied thermal boundary conditions associated with the isothermal curing were similar to those of the actual curing (see Section 4). Therefore, during the isothermal curing, the temperature within the composite was homogeneous. However, when the subsequent cooling started, due to the generated temperature difference and consequently the heat diffusion, the temperature distribution at the composite's microscale was not homogeneous.

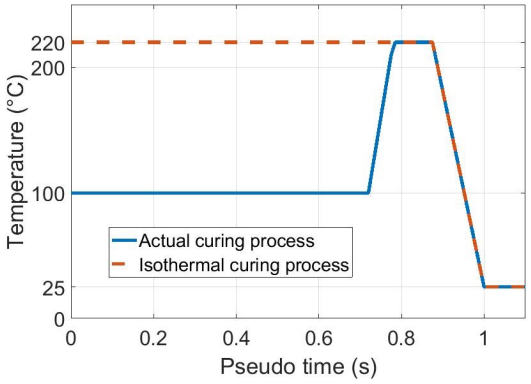

Fig. 10 Two possible scenarios for the curing process.

Figure 11 compares our three numerical analyses against the experimental data: (1) mechanical-only analysis, wherein no thermal curing was considered, (2) and (3) thermo-mechanical analyses with considering actual and isothermal curing processes, respectively, as presented in Figure 10. Figure 11 displays the tensile strengths of different microstructural realizations of the composite obtained by our different simulations with three box plots indicating average,

median, quartiles, and whiskers. In addition, this figure shows the average (red dashed line) and the range (shaded blue) of tensile strengths reported in the experiments of [4]. Note that the tensile strength corresponds to the maximum stress in the global stress-strain curve obtained for each realization.

As seen in Figure 11, the average strength calculated by the thermo-mechanical simulation with actual curing is much less than that by the mechanical-only simulation and much closer to the average strength of the experiment. It can be also observed that the average strength of the cured DFRC with the isothermal case is decreased by 20% compared to that of the uncured DFRC, i.e., the mechanical-only analysis. The reduction in overall strength can be explained by the fact that thermal curing processes can potentially introduce damage and fracture at the micro-scale level, affecting the global mechanical response of the composite. In Section 6.1, by performing parametric studies, we show that thermal curing processes may induce damage at the composite's microscale and, consequently, lead to reducing the overall strength of the composite structure. Also, in Section 6.2, we present that the type of damage caused by isothermal curing, compared to that caused by the actual curing, can greatly reduce the load-carrying capacity and the overall strength of the composite structure. The next section discusses the damage generated in the DFRC due to the actual curing procedure.

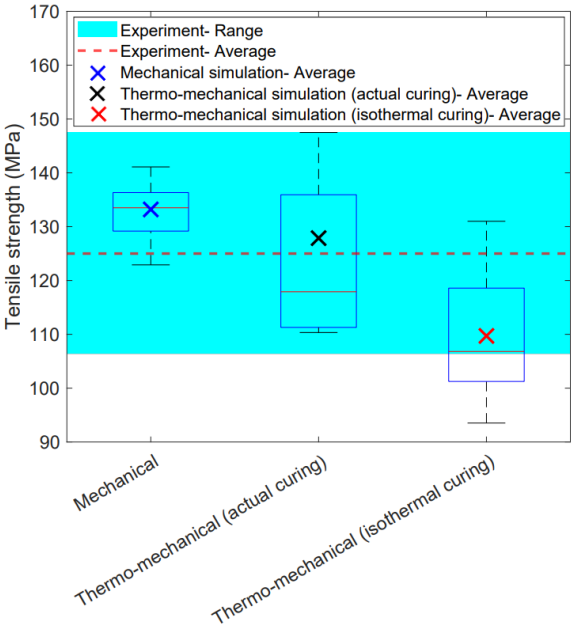

Fig. 11 Comparison of our thermo-mechanical and mechanical-only simulations' results for various microstructural realizations with the experimental data of [4]. In our thermo-mechanical analyses, two different curing processes were considered.

5.2 Formation of residual thermal stresses and damage due to curing

This section examines the induced residual thermal stresses and damage within the DFRC due to the actual curing process prior to the mechanical loading. The curing process considered in our analysis is according to the experimental data and shown in Figure 6. Figure 12(a) illustrates the von-Mises stresses at the end of the cooling stage, i.e., at the pseudo time of 1 s in Figure 10. Figure 12(b) and (c) displays the transverse and longitudinal cross-section views. It can be seen in Figure 12(b) that fibers sustain the high stress of 300 MPa, and the matrix tolerates the stress of around 20 MPa that happens near fibers' tips. As observed in Figure 12(c), the matrix at the fibers' tips sustains the highest stress (around 35 MPa) compared to the surrounding matrix. The 300 MPa stress within fibers is much smaller than the fibers' ultimate strength which is around 4 GPa [44], so the assumption that no fiber breakage happens was reasonable. The synergistic effects of several factors may cause the high-stress concentration within fibers: (1) the relatively high-temperature difference due to the heating and subsequent cooling procedures, (2) the intermediate FARs, (3) the very low fibers' volume fraction, and (4) consideration of the fibers' transverse thermal expansion in addition to their longitudinal thermal shrinkage in the 3-D analysis.

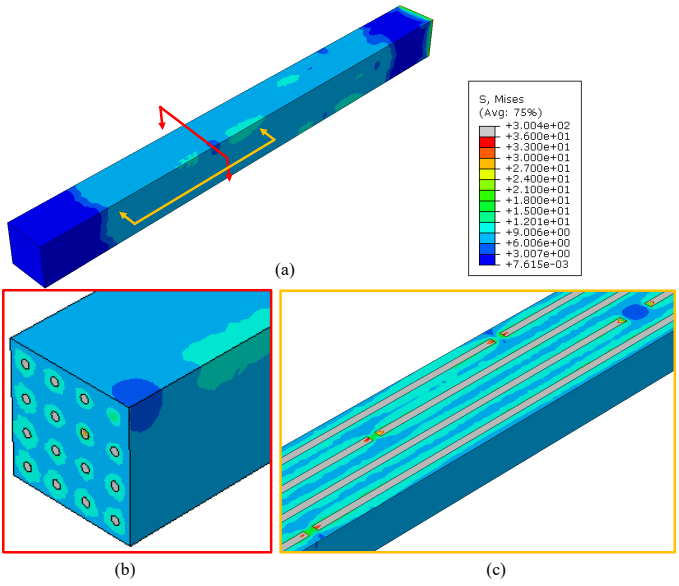

Fig. 12 (a) Residual thermal stresses at the end of the cooling stage. The transverse and longitudinal cross-section views are displayed in (b) and (c), respectively.

A combination of all the above factors has not been considered in the literature that simulated the curing-induced residual stresses in CFRCs. For

example, in [7], the von-Mises stresses within fibers were predicted to be around 100 MPa due to the relatively high curing temperature of 173°C; however, the fibers' volume fraction was 57%. For the matrix, we note that the observed maximum stress (i.e., around 35 MPa) was about a half of the matrix's strength and therefore was not enough for the generation of matrix cracking (see Figure 12(c)).

The high stresses generated due to the heating and subsequent cooling processes induced damage within the microstructure. Figure 13 shows the damage at the end of the curing process. It can be seen that the damage type is mainly the interface debonding type. Interface debondings occur due to the mismatch in the CTEs of matrix and fibers during the expansion and contraction processes. It is worth mentioning that under pure mechanical loading (i.e., without considering the thermal curing), the interface debonding damage was first observed at the global stress of 30 MPa [27]. Several parametric studies in Section 6 will show that the damage type of matrix cracking is also possible to occur at the end of the heating and subsequent cooling procedures.

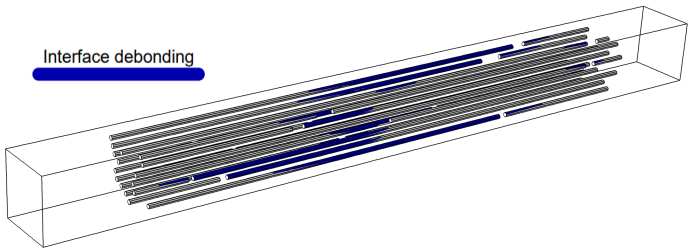

Fig. 13 Observed damage at the end of the curing process. The curing process induced interface debonding type of damage.

6 Parametric studies

This section presents several numerical tests to analyze the effects of curing-induced residual thermal stress on the mechanical response and the failure behavior of the DFRCs. A two-fiber microstructural representation containing two discontinuous aligned fibers, as shown in Figure 14, was utilized to effectively study the initiation of different damage types at the microscale (i.e., matrix damage and interface debonding). The two-fiber representation was found more useful than the previous large micromechanical representation to precisely observe the damage onset at the microscale because the high number of fibers in that micromechanical representation makes it difficult to explicitly capture the initiation stages of different damage types (see Figure 5). The two-fiber representation also reduces computational costs and provides the possibility of running several parametric studies. For the longitudinal loading and the low fibers' volume fraction scenarios in this work, the two-fiber case is

a reasonably simplified micromechanical representation that is useful for the engineering design of DFRCs.

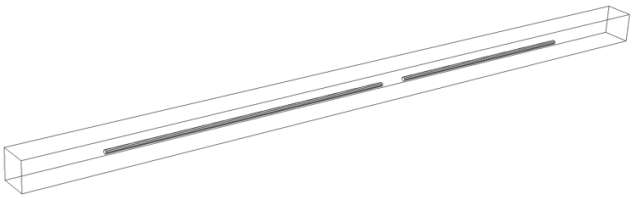

Fig. 14 The two-fiber microstructural representation used for parametric study.

The following subsections investigate the effects of curing temperature on the global stress-strain response and the local damage onset, the impacts of different curing processes on the beginning and evolution of different types of damage, and the influence of cohesive bonding versus perfect bonding for the fiber/matrix interface.

6.1 Effect of curing temperature on global mechanical response and damage initiation

The curing temperature plays an important role in polymer matrix composites' performance (e.g., [7]). This section examines the influence of different curing temperatures on the global stress-strain response and damage initiation of the DFRC. The curing temperatures were chosen from the range of 100°C to 220°C, as two prescribed curing temperatures in the experiment of [4]. The schematic illustration of isothermal heating and cooling processes from different curing temperatures to room temperature is drawn in Figure 15(a). The applied thermal boundary conditions are described in Section 5. After the curing procedure, a displacement-controlled mechanical load was applied. The schematic representations of the applied mechanical boundary conditions can be seen in Figures 1 and 2.

Figure 15(b) demonstrates the stress-strain curves under different curing temperatures until the final failure. These stress-strain curves were plotted after eliminating the stress-free shrinkage strains associated with the curing and cooling procedures, and the strains were calculated after the mechanical load was applied [46]. Figure 15(b) also includes the stress-strain curve of the case with no thermal curing being considered. As depicted in this figure, as the applied curing temperature increases, the overall strength (associated with the maximum stress) and toughness (associated with the area below the stress-strain curve) decrease. A similar observation was found in the experimental and numerical literature regarding the effects of curing temperature on the overall strength and toughness of other composite structures (woven, unidirectional, laminated, etc.) (e.g., [47–49]). However, in the literature studying the mechanical response of fiber-reinforced polymer matrix composites, we have

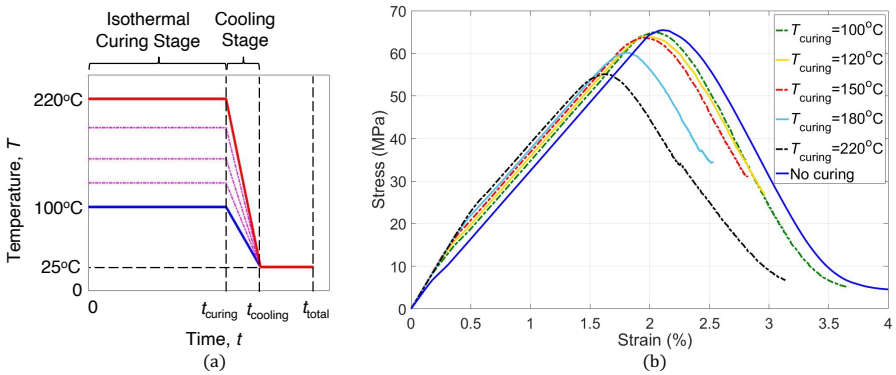

Fig. 15 (a) Schematic illustration of isothermal curing followed by cooling from different curing temperatures to room temperature, and (b) comparison of stress-strain curves under different isothermal curing shown in (a) including the curve with no curing.

not found a reference where the synergistic effects of all factors studied in our work were considered (see Section 5.2).

Based on our obtained results in Figure 15(b), the overall strength of the cured DFRC can be decreased by 20% (corresponding to the isothermal curing at 220°C) compared to that of the uncured DFRC. The same result was found in Section 5.1 using the previous large microstructural representation, justifying that the two-fiber representation used in the parametric studies was an appropriate selection for representing the DFRC. Owing to such differences between the results obtained by the thermo-mechanical analysis versus those by the mechanical-only one, we conclude that ignoring the effect of thermal curing procedures in the design and analysis of DFRCs may result in an unrealistic overestimation of the structure's ultimate strength and toughness.

The decrease in the overall strength and toughness can be explained by the hypothesis that as the applied curing temperature increases, damage at the microscale may grow, potentially leading to a decrease in the load-carrying capacity of the composite. Therefore, we study the effect of curing temperature on the damage initiation and accumulation prior to the mechanical loading. Figure 16 demonstrates the matrix damage occurring at the fibers' tips at the end of the cooling processes for different curing temperatures displayed in Figure 15(a). The obtained simulation results denote that there was no damage after the curing procedure with the temperature of 100°C. The matrix damage onset can be observed when the isothermal curing at 120°C was utilized. As seen in Figure 16, the matrix damage progresses when the applied curing temperature increases. The damage observed at the end of cooling is mainly due to the difference in the thermal properties of fiber and matrix constituents, which becomes more significant when the temperature difference (between curing temperature and room temperature) increases. In particular, the observed damage is predominately the result of the notable sign difference between the CTEs of the matrix and the fiber in the longitudinal direction

[46]. We conclude that high-temperature curing procedures can be detrimental to the overall composite's performance, as they can initiate damage and crack at the microscale, here in the form of matrix damage. Later, we show how curing procedures can initiate different damage types at the microscale.

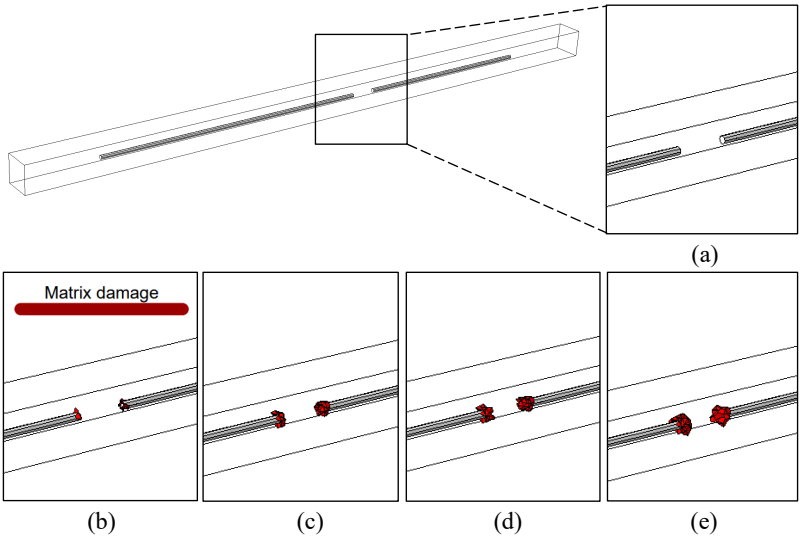

Fig. 16 Matrix damage at the fibers' tip at the end of the cooling stage for different curing temperatures of (a) 100°C, (b) 120°C, (c) 150°C, (d) 180°C, and (e) 220°C.

6.2 Effect of curing processes on initiation and propagation of different damage types

This section compares the effect of two possible scenarios for the curing process presented in Figure 10 followed by the same cooling process. The objective is to investigate if different curing procedures induce different types of damage in the composite.

Figures 17(a) and (b) illustrate the induced damage in the two-fiber microstructural representation after the two curing scenarios and before applying the mechanical loading. The subsequent heating and cooling in the actual curing causes subsequent expansion and contraction. Because of the notable difference between CTEs of the matrix and fibers, fibers move relative to the matrix [46]. The relative movement of fibers with respect to matrix escalates the debonding at the interfaces and leads to the initiation of debonding along fibers, in addition to the matrix damage at the fibers' tips (see Figure 17(a)). During the isothermal curing, due to the homogeneous temperature at the composite's microscale, the thermal strains of the fiber and the matrix are equal to zero (see Eq. 1). As the subsequent cooling begins, thermal strains of the composite's constituents start. The isothermal curing and its subsequent

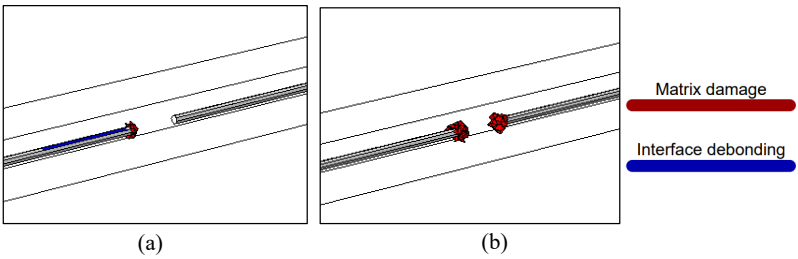

Fig. 17 Initiation of different damage types right after the end of two curing scenarios shown in Figure 10: (a) the actual curing (i.e., curing as in the experiment of [4]) led to both matrix damage and interface debonding, and (b) the isothermal curing led to only matrix damage.

cooling merely cause the matrix damage at fibers' tips (see Figures 17(b) or 16(e)). We hypothesize that in the isothermal curing case, having one cycle of temperature change (i.e., the cooling part), and therefore, fibers' relative movement to the matrix, was not enough to induce interfacial debonding. However, in the actual curing case, having two cycles of temperature change (i.e., the increase from 100° to 200° and the cooling part) induced bigger relative movement which caused substantial debonding. Also as observed in this figure, The matrix damage at fibers' ends formed due to the isothermal curing is more severe than that due to the actual curing.

We then study how these damage types progress with the exertion of mechanical loading. Figure 18 depicts the evolution of damage for the two-fiber microstructural representation up to the peak point of the stress-strain curve, respectively, for the actual and isothermal curing processes. The displayed failure pattern includes matrix damage and interface debonding. The damage evolution patterns associated with the isothermal curing at other temperatures exhibited in Figure 15 are not reported here since they demonstrated the similar pattern as those associated with the isothermal curing at 220°C seen in Figure 18(f)-(i).

The accumulation of matrix damage around fibers associated with the actual curing is more severe than that with the isothermal case (see Figure 18(d) and (i)). The reason for this observation in the damage evolution stage is related to the formation of the extra damage type of interfacial debonding due to the subsequent heating and cooling in the actual curing. The debonded interfacial zone propagated circumferentially along the interface and then kinked out inside the matrix. The coalescence of these kinked-out microcracks led to the development of matrix damage. That is because of the accepted fact that the mechanism of fiber/matrix interface failure has been known as the origin of transverse cracking in fiber-reinforced composites (e.g., [50]).

As seen in Figure 18(e) and (j), the peaks of stress-strain curves approximately are 64 MPa and 55 MPa, respectively, for the actual and isothermal curing scenarios. This difference denotes that the load-carrying capacity of the sample under the isothermal curing is lower than that under the actual curing.

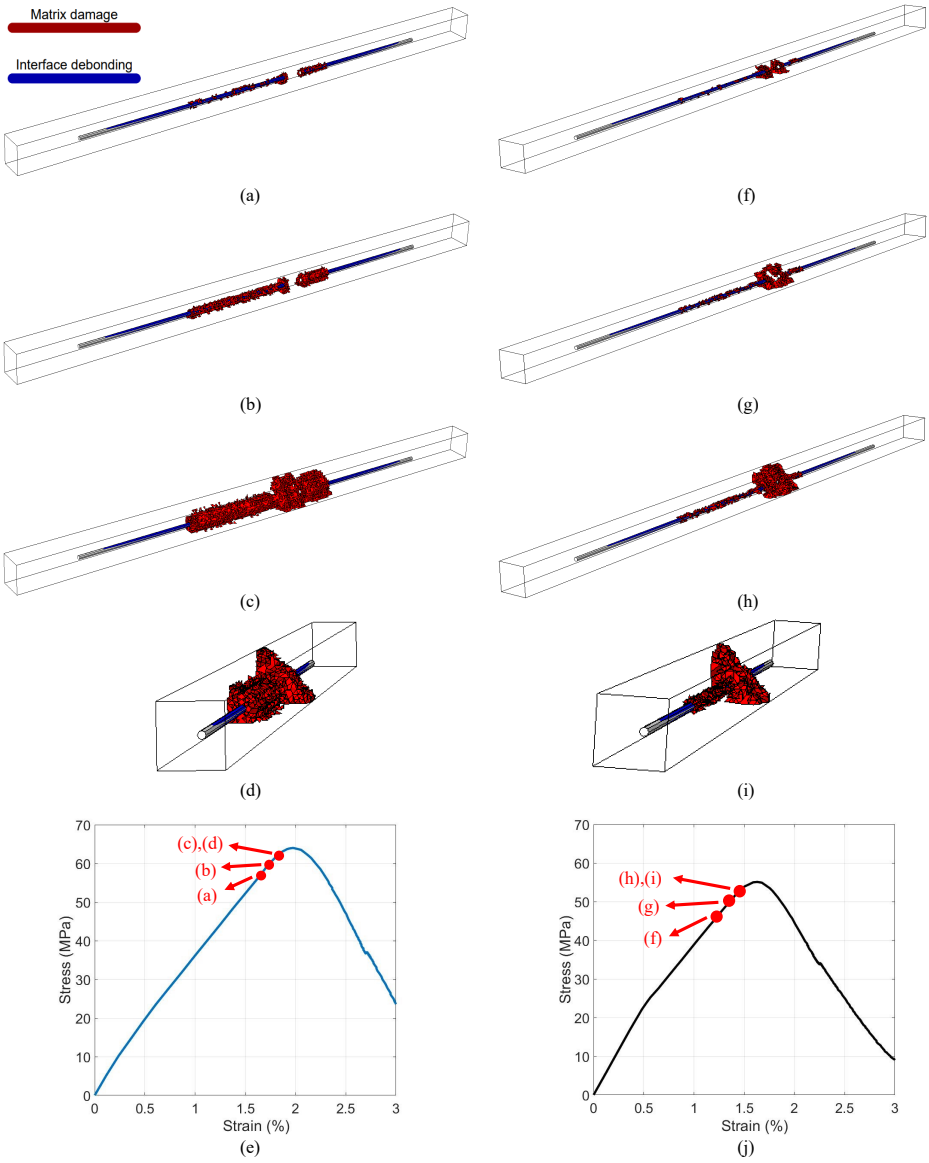

Fig. 18 (a)-(c) and (f)-(h) The evolution of damage and failure associated with, respectively, the actual curing (in the left column) and the isothermal curing at 220°C (in the right column), (d) and (i) another view of the damage map of (c) and (h), respectively, showing the damage progression through the cross-section, and (e) and (j) the stress-strain curves showing the loading stages immediately before the peak point, corresponding to the damage maps of (a)-(d) and (f)-(i), respectively.

This can be explained by this observation that, prior to applying the mechanical loading, the matrix damage at fibers' ends formed due to the isothermal curing was more severe than that due to the actual curing (see Figure 17). By applying the mechanical loading, the matrix damage evolved and propagated through the cross-section. Therefore, the sample undergone the isothermal curing reached the maximum load-carrying capacity at the lower stress, as the matrix damage between two fibers' ends propagated fully through the cross-section. Therefore, it is crucial to accurately consider curing procedures in analyzing the mechanical response and failure behavior in DFRCs because different curing procedures induce different forms of damage initiation and propagation.

The findings in this section revealed that the isothermal curing processes, compared to corresponding multi-stage curing processes, can be more detrimental to the overall mechanical performance, including the ultimate strength and toughness, of the composite structures. To this end, in general, multi-stage curing processes are more preferred and thus more frequently used in the literature (e.g., see [6, 7]). The next section studies the importance of accurately considering the fiber/matrix inferences in analyzing DFRCs.

6.3 Effect of cohesive versus perfect fiber/matrix interfacial bondings

This section compares the effect of the perfect versus cohesive interfacial bondings on the studied composite's performance. The fiber/matrix interface behavior in the simulations herein was considered based on the CZM described in Section 2.3.3. The perfect bonding case was considered by choosing very large values for the interfacial strength and fracture toughness. The actual curing was used in the thermo-mechanical analysis in this section (see Figure 6).

Figure 19(a) demonstrates different damage types near the fiber's end at the end of the cooling process and before applying the mechanical load. As observed in this figure, including the cohesive interfaces led to the initiation of both matrix damage and interface debonding. In contrast, the perfect interfaces resulted in the formation of only matrix damage. Also, in this figure, we observe that the matrix damage diminished by utilizing the perfect fiber/-matrix interface. Therefore, as expected, assuming perfect bonding interfaces underestimates the damage that happens at the microscale.

Figure 19(b) demonstrates the stress-strain curves for the cohesive versus perfect interfacial bondings once the mechanical load was applied after the actual curing procedure. As observed in this figure, utilizing the perfect bonding condition resulted in drastically lower overall strength and toughness for the composite structure compared to the case with the cohesive bonding condition. This observation can be explained by the possible formation of unexpected and catastrophic macrocracks in the composite structure. By assuming the perfect interfaces, damage at the microscale that would normally occur if the cohesive interfaces were assumed was prohibited from appearing

(see Figure 19(a)). This may cause sudden macrocracks to "pop up", leading to a reduction in the structure's ability to sustain and transmit the load and, ultimately, a decrease in the structure's strength and toughness.

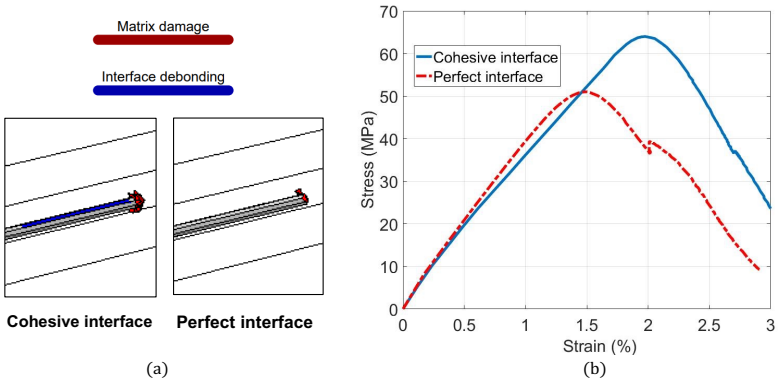

Fig. 19 (a) Different damage types near the fiber's end, at the end of the cooling process, and (b) stress-strain curves for the cohesive versus perfect fiber/matrix interfacial bondings. The curing and the subsequent cooling processes were as described in [4].

Figure 20 displays the evolution of damage and failure associated with the perfect fiber/matrix bonding. In comparison with the evolution of damage and failure associated with the cohesive interfacial bonding shown in Figure 18, the amount of matrix damage is considerably mitigated and concentrated more in the area between two fibers, rather than around each fiber. It can be concluded that utilization of perfect bonding causes an unrealistic underestimation in predicting both the overall strength and toughness and the damage/failure at the microscale. Therefore, it is highly crucial to consider the cohesive interface bonding in simulating the overall performance of DFRCs.

Most literature studying the curing-induced residual stresses in CFRCs assumed the perfect interfacial bonding, which only includes the fiber and matrix phases as the composite's constituents (e.g., ([21, 23, 24]). However, the constitutive equations with imperfect adhesion between the fiber and the matrix were found in the literature to be more realistic [51]. The reference [51] analytically studied the influence of imperfect fiber/matrix bonding on thermal residual stress fields in fiber-reinforced composites and found that utilizing the perfect bonding may result in a decline in the ability to sustain and transmit the load. Therefore, the observation in Figure 19(b) agrees well with the theoretical investigations in [51].

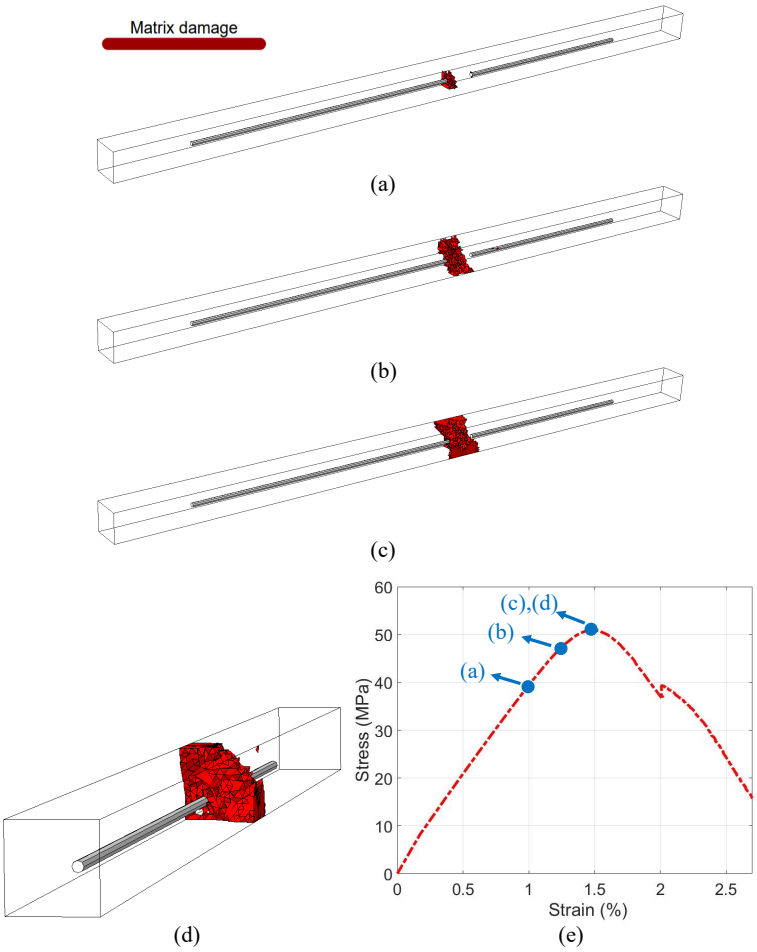

Fig. 20 (a)-(c) The evolution of damage and failure associated with the perfect fiber/matrix interfacial bonding. (d) is another view of the damage map of (c), showing the damage progression through the cross-section, and (e) the stress-strain curve showing the loading stages immediately before the peak point, corresponding to the damage maps of (a)-(c).

7 Concluding remarks and future work

In this work, we investigated the effects of residual thermal stresses due to curing procedures on the mechanical response and the failure behavior of additively manufactured aligned DFRCs. The main conclusions can be summarized as follows:

- The fibers' tips sustain higher residual thermal stresses than the surrounding matrix, potentially leading to matrix damage prior to mechanical loading.

- The onset of matrix damage at the fibers' tips was observed due to the isothermal curing at 120°C before any mechanical loading–damage accumulated with the increase of the applied curing temperature.
- With increasing the applied curing temperature, the overall strength and toughness decreased. The overall strength of the cured DFRC was reduced by 20% (associated with the isothermal curing at 220°C) compared to that of the uncured DFRC (associated with pure mechanical analysis).
- By assuming two curing processes, it was found that the curing, according to the experiment, led to the formation of both interface debonding and matrix damage. In contrast, the isothermal curing resulted in the formation of matrix damage.
- Utilizing perfect, rather than cohesive, interfacial bonding caused an unrealistic underestimation in predicting the overall strength and toughness and the damage/failure at the microscale. Thus, it is crucial to consider the cohesive interface bonding to simulate the DFRC's response.

This work provides some guidance on the curing procedure of additively manufactured aligned DFRCs which will eventually lead to better design, manufacturing, and analysis of such composites. In the future, more detailed information on the possible cure-dependent and temperature-dependent behavior of each composite's constituent will be extracted and implemented into the modeling framework to comprehensively simulate the effects of thermal curing on the mechanical response and damage behaviour of such composites.

Acknowledgment. The authors gratefully acknowledge the support from the Air-Force Office of Scientific Research (AFOSR) Young Investigator Program (YIP) award (Award No. FA9550-20-1-0281). The authors also acknowledge Advanced Research Computing at Virginia Tech for providing computational resources and technical support that have contributed to the results reported within this paper.

Data Availability

The datasets generated during and/or analysed during the current study are available on reasonable request.

Appendix A On alleviating mesh-dependency in the damage constitutive framework

It is well-known that after the initiation of damage/microcracks within materials, they usually exhibits a softening behavior in their macroscopic stress-strain response, leading to strain localization [52, 53]. Within a traditional finite element framework, this issue would introduce a strong mesh dependency into the results. However, recently in ABAQUS, the damage evolution law in the utilized plasticity damage constitutive framework uses a formulation intended to

greatly alleviate the mesh dependency [28]. This is accomplished by implementing Hillerborg's (1976) fracture energy proposal that introduces a characteristic length, L, into the formulation and expresses the softening part of the constitutive law as a stress-displacement, rather than stress-strain, relation (see [54]). For example, for 2-D elements, the characteristic length is described as the square root of the average area of the mesh elements [28]. Once the damage initiation or yield criterion is met, the evolution of the damage variable is defined as the ratio of the effective plastic displacement rate, $\dot{u}_{pl}$, to the effective plastic displacement at the complete material failure, u^f_{pl}, as

$$\dot{d} = \frac{L\dot{\epsilon}_{pl}}{u^f_{pl}} = \frac{\dot{u}_{pl}}{u^f_{pl}} \tag{A1}$$

For more information on the damage constitutive framework, readers are referred to [28, 35, 37].

References

[1] Tekinalp, H., Kunc, V., Velez-Garcia, G., Duty, C., Love, L., Naskar, A., Blue, C. & Ozcan, S. Highly oriented carbon fiber–polymer composites via additive manufacturing. *Composites Science and Technology.* **105** pp. 144-150 (2014)

[2] Compton, B. & Lewis, J. 3D-printing of lightweight cellular composites. *Advanced Materials.* **26**, 5930-5935 (2014)

[3] Lewicki, J., Rodriguez, J., Zhu, C., Worsley, M., Wu, A., Kanarska, Y., Horn, J., Duoss, E., Ortega, J., Elmer, W. & Others 3D-printing of meso-structurally ordered carbon fiber/polymer composites with unprecedented orthotropic physical properties. *Scientific Reports.* **7**, 1-14 (2017)

[4] Pierson, H., Celik, E., Abbott, A., De Jarnette, H., Sierra Gutierrez, L., Johnson, K., Koerner, H. & Baur, J. Mechanical properties of printed epoxy-carbon fiber composites. *Experimental Mechanics.* **59**, 843-857 (2019)

[5] Yang, L., Yan, Y., Ma, J. & Liu, B. Effects of inter-fiber spacing and thermal residual stress on transverse failure of fiber-reinforced polymer–matrix composites. *Computational Materials Science.* **68** pp. 255-262 (2013)

[6] Danzi, F., Fanteria, D., Panettieri, E. & Mancino, M. A numerical micro-mechanical study on damage induced by the curing process in carbon/epoxy unidirectional material. *Composite Structures.* **210** pp. 755-766 (2019)

[7] Hui, X., Xu, Y. & Zhang, W. An integrated modeling of the curing process and transverse tensile damage of unidirectional CFRP composites.

Composite Structures. **263** pp. 113681 (2021)

[8] Nairn, J. & Zoller, P. Matrix solidification and the resulting residual thermal stresses in composites. *Journal of Materials Science.* **20**, 355-367 (1985)

[9] Parlevliet, P., Bersee, H. & Beukers, A. Residual stresses in thermoplastic composites—A study of the literature—Part I: Formation of residual stresses. *Composites Part A: Applied Science and Manufacturing.* **37**, 1847-1857 (2006)

[10] Parlevliet, P., Bersee, H. & Beukers, A. Residual stresses in thermoplastic composites—A study of the literature—Part II: Experimental techniques. *Composites Part A: Applied Science and Manufacturing.* **38**, 651-665 (2007)

[11] Bogetti, T. & Gillespie Jr, J. Process-Induced Stress and Deformation in Thick-Section Thermoset Composite Laminates. *Journal of Composite Materials.* **26**, 626-660 (1992)

[12] Cowley, K. & Beaumont, P. The measurement and prediction of residual stresses in carbon-fibre/polymer composites. *Composites Science and Technology.* **57**, 1445-1455 (1997)

[13] Olivier, P. & Cottu, J. Optimisation of the co-curing of two different composites with the aim of minimising residual curing stress levels. *Composites Science and Technology.* **58**, 645-651 (1998)

[14] Gopal, A., Adali, S. & Verijenko, V. Optimal temperature profiles for minimum residual stress in the cure process of polymer composites. *Composite Structures.* **48**, 99-106 (2000)

[15] Chen, W. & Zhang, D. A micromechanics-based processing model for predicting residual stress in fiber-reinforced polymer matrix composites. *Composite Structures.* **204** pp. 153-166 (2018)

[16] Sweeting, R. & Thomson, R. The effect of thermal mismatch on Z-pinned laminated composite structures. *Composite Structures.* **66**, 189-195 (2004)

[17] Zhang, Y., Xia, Z. & Ellyin, F. Evolution and influence of residual stresses/strains of fiber reinforced laminates. *Composites Science and Technology.* **64**, 1613-1621 (2004)

[18] Zhao, L., Warrior, N. & Long, A. A micromechanical study of residual stress and its effect on transverse failure in polymer–matrix composites. *International Journal of Solids and Structures.* **43**, 5449-5467 (2006)

[19] Zhao, L., Warrior, N. & Long, A. A thermo-viscoelastic analysis of process-induced residual stress in fibre-reinforced polymer–matrix composites. *Materials Science and Engineering: A*. **452-453** pp. 483-498 (2007)

[20] Jia, Y., Yan, W. & Liu, H. Carbon fibre pullout under the influence of residual thermal stresses in polymer matrix composites. *Computational Materials Science*. **62** pp. 79-86 (2012)

[21] D'Mello, R., Maiarù, M. & Waas, A. Effect of the curing process on the transverse tensile strength of fiber-reinforced polymer matrix lamina using micromechanics computations. *Integrating Materials and Manufacturing Innovation*. **4**, 119-136 (2015)

[22] Yuan, Z., Wang, Y., Yang, G., Tang, A., Yang, Z., Li, S., Li, Y. & Song, D. Evolution of curing residual stresses in composite using multi-scale method. *Composites Part B: Engineering*. **155** pp. 49-61 (2018)

[23] Shah, S. & Maiarù, M. Effect of Manufacturing on the Transverse Response of Polymer Matrix Composites. *Polymers*. **13**, 2491 (2021)

[24] Shah, S., Patil, S., Hansen, C., Odegard, G. & Maiarù, M. Process modeling and characterization of thermoset composites for residual stress prediction. *Mechanics of Advanced Materials and Structures*. pp. 1-12 (2021)

[25] Hernandez, L., Sepasdar, R. & Shakiba, M. Sensitivity of crack formation in fiberreinforced composites to microstructural geometry and interfacial properties. *Proceeding of The American Society for Composites, Thirty-Fifth Technical Conference*. pp. 1576-1591 (2020)

[26] Shakiba, M. Detecting Transverse Cracks Initiation in Composite Laminates via Statistical Analysis of Sensitivity Data. *Mechanics Research Communications*. pp. 103701 (2021)

[27] Sepasdar, R., Niazi, S., Case, S. & Shakiba, M. A 3-D Micro-Mechanical Framework to Study Damage Propagation and Failure of Printed Discontinuous Fiber-Reinforced Composites. *Submitted*. (2022)

[28] Systèmes, D. ABAQUS 6.10: Analysis user's manual. *Providence, RI: Dassault Systèmes Simulia Corp*. (2010)

[29] Li, C., Potter, K., Wisnom, M. & Stringer, G. In-situ measurement of chemical shrinkage of MY750 epoxy resin by a novel gravimetric method. *Composites Science and Technology*. **64**, 55-64 (2004)

[30] Yu, H., Mhaisalkar, S. & Wong, E. Cure shrinkage measurement of non-conductive adhesives by means of a thermomechanical analyzer. *Journal of Electronic Materials*. **34**, 1177-1182 (2005)

[31] Khoun, L., Centea, T. & Hubert, P. Characterization methodology of thermoset resins for the processing of composite materials—case study: CYCOM 890RTM epoxy resin. *Journal of Composite Materials*. **44**, 1397-1415 (2010)

[32] Tu, W. & Chen, Q. Evolution of interfacial debonding of a unidirectional graphite/polyimide composite under off-axis loading. *Engineering Fracture Mechanics*. **230** pp. 106947 (2020)

[33] Sepasdar, R., Karpatne, A. & Shakiba, M. A Data-Driven Approach to Full-Field Damage and Failure Pattern Prediction in Microstructure-Dependent Composites using Deep Learning. *Computer Methods in Applied Mechanics and Engineering*. **397** pp. 115126 (2022)

[34] Sepasdar, R. & Shakiba, M. Micromechanical study of multiple transverse cracking in cross-ply fiber-reinforced composite laminates. *Composite Structures*. **281** pp. 114986 (2022)

[35] Lubliner, J., Oliver, J., Oller, S. & Oñate, E. A plastic-damage model for concrete. *International Journal of Solids and Structures*. **25**, 299-326 (1989)

[36] Lee, J. & Fenves, G. Plastic-damage model for cyclic loading of concrete structures. *Journal Of Engineering Mechanics*. **124**, 892-900 (1998)

[37] Vaughan, T. & McCarthy, C. Micromechanical modelling of the transverse damage behaviour in fibre reinforced composites. *Composites Science and Technology*. **71**, 388-396 (2011)

[38] Canal, L., González, C., Segurado, J. & LLorca, J. Intraply fracture of fiber-reinforced composites: Microscopic mechanisms and modeling. *Composites Science and Technology*. **72**, 1223-1232 (2012)

[39] Herráez, M., Mora, D., Naya, F., Lopes, C., González, C. & LLorca, J. Transverse cracking of cross-ply laminates: A computational micromechanics perspective. *Composites Science and Technology*. **110** pp. 196-204 (2015)

[40] Herráez, M., González, C. & Lopes, C. A numerical framework to analyze fracture in composite materials: From R-curves to homogenized softening laws. *International Journal of Solids and Structures*. **134** pp. 216-228 (2018)

[41] Sepasdar, R. & Shakiba, M. Overcoming the convergence difficulty of cohesive zone models through a Newton-Raphson modification technique. *Engineering Fracture Mechanics.* **233** pp. 107046 (2020)

[42] Gao, Y. & Bower, A. A simple technique for avoiding convergence problems in finite element simulations of crack nucleation and growth on cohesive interfaces. *Modelling and Simulation in Materials Science and Engineering.* **12**, 453-463 (2004)

[43] Cheng, H., Gao, J., Kafka, O., Zhang, K., Luo, B. & Liu, W. A micro-scale cutting model for UD CFRP composites with thermo-mechanical coupling. *Composites Science and Technology.* **153** pp. 18-31 (2017)

[44] Hyer, M. & White, S. Stress Analysis of Fiber-reinforced Composite Materials. (DEStech Publications, Inc, 2009)

[45] Hernandez, D., Soufen, C. & Orlandi, M. Carbon fiber reinforced polymer and epoxy adhesive tensile test failure analysis using scanning electron microscopy. *Materials Research.* **20** pp. 951-961 (2017)

[46] Niazi, S., Najmeddine, A. & Shakiba, M. A 3D thermo-mechanical analysis of additively manufactured aligned discontinuous fiber-reinforced composites. *Proceeding of The American Society for Composites, Thirty-Seventh Technical Conference.* pp. 1292-1311 (2022)

[47] Gentz, M., Armentrout, D., Rupnowski, P., Kumosa, L., Shin, E., Sutter, J. & Kumosa, M. In-plane shear testing of medium and high modulus woven graphite fiber reinforced/polyimide composites. *Composites Science and Technology.* **64**, 203-220 (2004)

[48] Gentz, M., Benedikt, B., Sutter, J. & Kumosa, M. Residual stresses in unidirectional graphite fiber/polyimide composites as a function of aging. *Composites Science and Technology.* **64**, 1671-1677 (2004)

[49] Chen, Q., Chen, X., Zhai, Z., Zhu, X. & Yang, Z. Micromechanical modeling of viscoplastic behavior of laminated polymer composites with thermal residual stress effect. *Journal of Engineering Materials and Technology.* **138**, 031005 (2016)

[50] Livingston, R. & Koohbor, B. Characterizing fiber-matrix debond and fiber interaction mechanisms by full-field measurements. *Composites Part C.* **7** pp. 100229 (2022)

[51] Shokrieh, M. & Safarabadi, M. Effects of imperfect adhesion on thermal micro-residual stresses in polymer matrix composites. *International Journal of Adhesion and Adhesives.* **31**, 490-497 (2011)

[52] Niazi, S., Chen, Z. & Bobaru, F. Crack nucleation in brittle and quasi-brittle materials: A peridynamic analysis. *Theoretical and Applied Fracture Mechanics*. **112** pp. 102855 (2021)

[53] Niazi, S. Peridynamic Models for Crack Nucleation in Brittle and Quasi-Brittle Materials. (Doctoral dissertation, The University of Nebraska-Lincoln, Dec. 2020)

[54] Hillerborg, A., Modéer, M. & Petersson, P. Analysis of crack formation and crack growth in concrete by means of fracture mechanics and finite elements. *Cement and Concrete Research*. **6**, 773-781 (1976)